Thin-film preparation and characterization of $Cs_3Sb_2I_9$: A lead-free layered perovskite semiconductor

Bayrammurad Saparov[1,2], Feng Hong[3,4], Jon-Paul Sun,[5] Hsin-Sheng Duan[1], Weiwei Meng[3], Samuel Cameron,[5] Ian G. Hill,[5] Yanfa Yan[3],* David B. Mitzi[1,2] *

[1]Department of Mechanical Engineering and Materials Science, Duke University, Durham, NC 27708, USA

[2]Department of Chemistry, Duke University, Durham, NC 27708, USA

[3]Department of Physics and Astronomy and Center for Photovoltaics Innovation and Commercialization, The University of Toledo, Toledo, Ohio 43606, USA

[4]Department of Physics, Shanghai University, Shanghai 200444, China

[5]Department of Physics and Atmospheric Science, Dalhousie University, Halifax, Nova Scotia B3H 3J5, Canada

* Corresponding authors: yanfa.yan@utoledo.edu, david.mitzi@duke.edu

Supporting Information

Disclaimer: The information, data, or work presented herein was funded in part by an agency of the United States Government. Neither the United States Government nor any agency thereof, nor any of their employees, makes any warranty, express or implied, or assumes any legal liability or responsibility for the accuracy, completeness, or usefulness of any information, apparatus, product, or process disclosed, or represents that its use would not infringe privately owned rights. Reference herein to any specific commercial product, process, or service by trade name, trademark, manufacturer, or otherwise does not necessarily constitute or imply its endorsement, recommendation, or favoring by the United States Government or any agency thereof. The views and opinions of authors expressed herein do not necessarily state or reflect those of the United States Government or any agency thereof.

Bulk syntheses of the dimer and layered forms of $Cs_3Sb_2I_9$: The dimer form of $Cs_3Sb_2I_9$ (Figure S1) is obtained through reactions of CsI and SbI_3 in stoichiometric 3:2 ratios in polar solvents (acetonitrile, N,N-dimethylformamide (DMF), etc.). The solubility of the reaction mixture was found to be highest in DMF. Due to air/moisture-sensitivity of reactants, all manipulations were carried out inside a nitrogen-filled glovebox. Reactants (14 mg of CsI and 18 mg of SbI_3) were weighed in a nitrogen-filled glovebox; 3 ml DMF was added and the solution was stirred for 30 minutes to form an orange solution. Evaporation of this solution affords the dimer modification of $Cs_3Sb_2I_9$ in pure form. The dimer form of $Cs_3Sb_2I_9$ has an intense orange color, and is stable under ambient air if left out overnight. Note that according to literature,[1] the dimer or layered forms can be obtained depending on the polarity of the solvent used. In certain cases, then, it can be speculated that a mixture of two phases could occur; however, since many diffraction peaks for the two modifications coincide (see Figure 3 and Figure S2 for simulated patterns), quantifying the mixture content is often difficult.

X-ray diffraction of the dimer modification of $Cs_3Sb_2I_9$ obtained from evaporation of the DMF solution is provided in Figure S2. We attempted to transform the dimer form into the layered form by annealing it at 250 °C, following the literature description.[1] However, annealing the dimer form inside a quartz cup (not a hermetically sealed reaction vessel) does not result in formation of the layered modification. Instead, SbI_3 evaporates, leaving behind an excess of CsI. Evolution of CsI peaks is clearly visible in the GIXRD patterns, and longer anneal times increase intensities of the CsI peaks. The failure to reproduce the literature data is due to the fact that the annealing step

was not carried out in an enclosed reaction vessel. Inside a sealed container, the dimer form completely decomposes into CsI and SbI_3 and, upon cooling, these compounds undergo a gas-solid reaction to form the layered structure. This conjecture is supported by the fact that reactions carried out at 250 °C-350 °C between CsI and intentionally introduced SbI_3 vapor indeed result in the formation of the layered $Cs_3Sb_2I_9$.

The layered polymorph of $Cs_3Sb_2I_9$ can be obtained through solid state or gas phase reactions. In bulk form, the layered $Cs_3Sb_2I_9$ was obtained by reacting a stoichiometric mixture of CsI and SbI_3 in two steps. First, the finely ground mixture was cold-pressed into a pellet, and annealed at 140 °C for two hours inside an unsealed quartz cup. This step is necessary to avoid excessive losses of the volatile reactant SbI_3 (T_{mp} = 171 °C). After this first annealing step, the pellet changed from its initial orange color to a red color, indicating a substantial reaction occurring at 140 °C. To improve crystallinity, the pellet was then annealed at 250 °C for 2 hours inside the unsealed quartz cup. After the second annealing step, the color of the pellet darkens further.

Preferentially c-axis oriented layered $Cs_3Sb_2I_9$ thin-film deposition: Highly-oriented layered $Cs_3Sb_2I_9$ thin-films were fabricated through co-evaporation of CsI and SbI_3 using Radak sources in an Angstrom Engineering evaporator (base pressure = ~5×10^{-7} Torr). During co-evaporation, the deposition rates are kept close to $r(CsI)/r(SbI_3) \sim 1.43$, with the targeted final thickness of typically 300 nm. The co-evaporated films, then, are annealed in SbI_3 vapor inside a N_2-filled glove-box and under a quartz cover to avoid SbI_3 loss from the reaction medium. With the subsequent annealing step, the final thicknesses of annealed co-evaporated films range from 380-440 nm, depending on the evaporation and annealing conditions.

For thermal treatment, a hot plate is set at a desired temperature and left to stabilize at this temperature. Then, co-evaporated films are put onto the hot plate (center of the hot plate, avoiding the corners) together with a glass slide with SbI_3 powder on top, and quickly covered with a quartz cover. In several cases, a glass slide with drops of DMF on top (several droplets measuring ~2-6 µL) are also brought under the quartz cover. We note that during our annealing experiments without a quartz cover, a considerable amount of SbI_3 was lost from the film, and consequently, a large amount of CsI impurity was present in the resultant film. The evaporation of SbI_3 powder is gradual, and the thermal equilibrium is reached in 5-10 minutes. Following the annealing step, the thin-films are quenched. Quenching from above 250 °C may lead to a partial evaporation of SbI_3

from the films, leaving behind unreacted CsI; therefore, it is safer to quench after cooling the films to 200 °C.

Randomly-oriented layered $Cs_3Sb_2I_9$ thin-film deposition: To obtain randomly-oriented $Cs_3Sb_2I_9$ thin-films, the CsI and SbI_3 reaction must occur rapidly. In order to achieve this, a sequential deposition, which involves deposition of a CsI film through evaporation, followed by annealing in SbI_3 vapor, was found to be the best method. For this purpose, CsI films (150 nm) were deposited in the evaporator using a Radak source. To ensure a rapid reaction, SbI_3 powder is brought under a quartz cover at the desired annealing temperature and left to stabilize at this temperature (5-10 minutes). After thermal stabilization of SbI_3 vapor (i.e., pre-heated SbI_3 vapor) and quartz cover at this temperature, CsI films are quickly brought under the quartz cover and annealed for up to 1 hour. The resultant randomly-oriented films with film thicknesses the same as mentioned above are quenched after cooling to 200 °C on top of a hot plate.

The temperature dependence of SbI_3 vapor pressure has been extensively studied in literature.[2, 3] At lower annealing temperature of 250 °C, the vapor pressure is in 20-30 mm Hg range, whereas at 300 °C, the vapor pressure increases to 75-90 mm Hg. At 350 °C, the vapor pressure is ~295 mm Hg.

Characterization of thin films: FEI XL30 Scanning Electron Microscopy (SEM) was used to obtain high resolution images of the fabricated thin-films. Optical absorption measurements were carried out on a Shimadzu UV-3600 spectrophotometer. Photoluminescence measurements were performed on a Horiba Jobi- Yvon LabRAM ARAMIS system using a 442 nm laser excitation. The best spectra for $Cs_3Sb_2I_9$ were obtained by filtering 90-99% of the incoming laser energy intensity (laser power at the sample surface kept below 100 µW, as measured by a power meter), with exposure times less than 5 seconds and with a 10× objective. Prolonged exposure to the laser or the use of higher laser intensity leads to a gradual decrease of the PL peak intensity (see Figure S5). Eventually, this leads to a complete decomposition of $Cs_3Sb_2I_9$, as evidenced by a visible hole on the measurement spot and a complete disappearance of the $Cs_3Sb_2I_9$ PL peak at 633 nm. For comparison of PL spectra, a methylammonium lead iodide ($CH_3NH_3PbI_3$) film was fabricated on a glass slide by spin coating, using a 3:1 ratio of methylammonium iodide (MAI) and lead chloride ($PbCl_2$) starting materials in DMF.[4] The $CH_3NH_3PbI_3$ film is also susceptible to laser damage[5] and, therefore, similar conditions were used for PL measurement experiments.

X-ray diffraction measurements were performed on a PANalytical Empyrean powder X-ray diffractometer. The X-ray diffraction experiments were carried out under ambient conditions. Air-stability of the thin films was investigated by leaving them in a dark cabinet outside in ambient air with a day-to-day relative humidity fluctuation ranging from 20 to 50%. For most days, the humidity values fluctuated from 20 to 30%; however, increases above 40% were also noted. A methylammonium lead iodide ($CH_3NH_3PbI_3$) film was fabricated using a 3:1 ratio of methylammonium iodide (MAI) and lead chloride ($PbCl_2$) starting materials in DMF for a direct comparison of stabilities under moist air (see Figure S4). For this purpose, the precursors were kept at 60 °C prior to spin-coating on a compact TiO_2/FTO substrate at 2000 rpm for 60 s. The spin-coated film was dried at room temperature for 30 min, followed by annealing at 75 °C (10 min) and 90 °C (1 h). The use of a compact TiO_2/FTO substrate is necessary in order to obtain a smooth, impurity free thin film. The $CH_3NH_3PbI_3$ film decomposition is clearly visible in the low angle region as an increase in the PbI_2 impurity peak intensity. Additionally, a small amount of leftover $CH_3NH_3PbCl_3$ impurity is seen. There is another strong peak that emerges below 10° (at 7.30°), which most likely indicates the formation of $CH_3NH_3PbI_3$ monohydrate.[6-8] It has been reported that the hydration-dehydration process is reversible, and that one can observe diffraction peaks at 7.93°, 8.42°, 10.46°, and 16.01° depending on the storing conditions (humidity and the storage time) of the $CH_3NH_3PbI_3$ film,[7] suggesting possible formation of other products of hydration. Humidity levels of 60% have been recognized as a threshold where the films degrade completely.[6] Under our storing conditions, we observe the emergence of what is presumably the $CH_3NH_3PbI_3{\cdot}H_2O$ peak first,[4-6] which gradually decreases in the intensity over time, and simultaneously the PbI_2 impurity peak increases. It should also be noted that, under humid air, the $CH_3NH_3PbI_3$ peaks become sharper with full width at half maximum (FWHM) going from 0.197° to 0.095°, which is attributed to the improvement of crystallinity under the presence of solvent (moist air) and is not unexpected.[9]

Solar cell device fabrication: Fluorine-doped tin oxide coated glass (FTO, Sigma-Aldrich, surface resistivity 7 Ω/□) was patterned by etching with a 2 M HCl solution and Zn powder. The substrates were then cleaned using deionized water and sonicated in acetone, ethanol and isopropanol (IPA, Sigma-Aldrich) for 10 minutes each. The compact layer of TiO_2 was deposited via spin coating at 2000 rpm for 1 min using a precursor solution of 0.23 M Ti (IV) isopropoxide (Sigma-Aldrich) and 0.013 M HCl in IPA. After spin coating, the substrates were annealed in air at 520 ºC on a hot

plate for 1 h. This was followed by $Cs_3Sb_2I_9$ thin-film deposition, described above in detail. The hole transport material (HTM) solution consisted of 10 mg poly[bis(4-phenyl)(2,4,6-trimethylphenyl)amine] (PTAA, Lumtec, MW > 10,000) in 1 ml toluene, 7.5 µl Li-bis(trifluoromethanesulfonyl) imide (Li-TFSI)/acetonitrile (170 mg/ml) and 4 µl 4-tert-butylpiridine (tBP). The HTM solution was spin-coated inside the glovebox at 3000 rpm for 30 s on the $Cs_3Sb_2I_9$ films. Finally, 80 nm-thick gold contacts were deposited by thermal evaporation.

The devices with preferentially- and randomly-oriented films do not show appreciable difference in performance. The devices demonstrate open-circuit voltages of up to V_{oc} = 300 meV; however, the short-circuit current densities J_{sc} remain low (< 0.1 mA/cm^2), resulting in low device efficiencies. The evaluation of hysteresis is difficult under these conditions of low performance; however, based on our device data, forward and reverse scans give similar results (Figure S13).

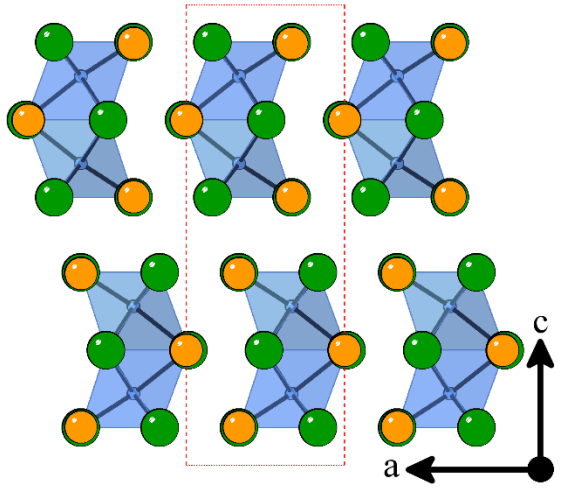

Figure S1. The crystal structure of the dimer modification of $Cs_3Sb_2I_9$ is made of $Sb_2I_9^{3-}$ anions separated by Cs^+ cations. Cs and I atoms are shown as orange and green spheres, respectively; Sb coordination polyhedra are shown in blue.

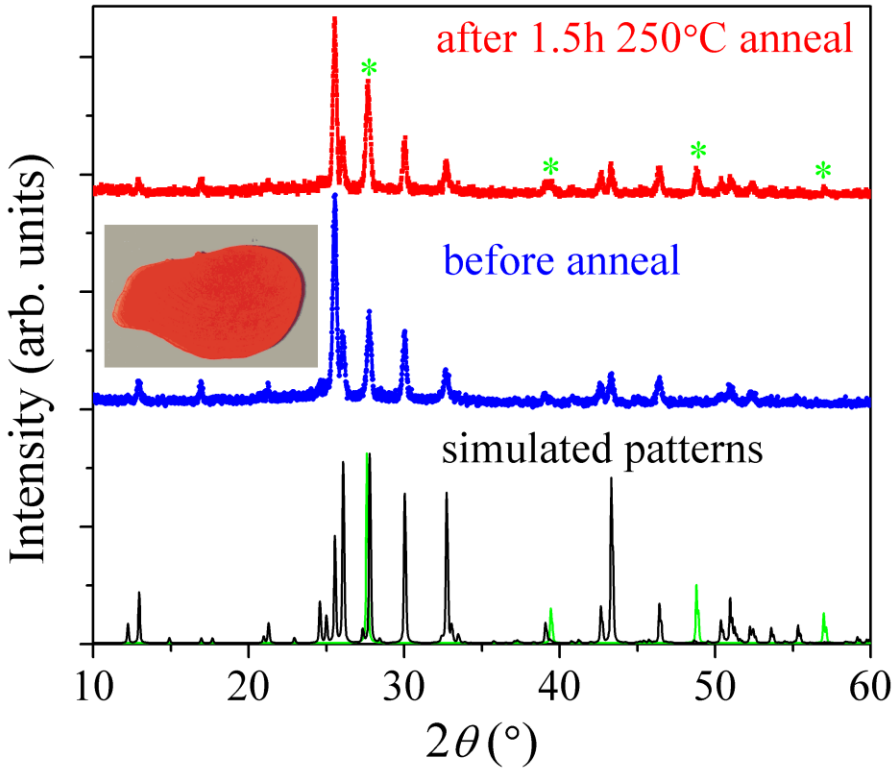

Figure S2. X-ray diffraction patterns of the *P*6$_3$/*mmc* dimer modification of $Cs_3Sb_2I_9$ before (blue) and after (red) annealing at 250 °C. After the heat treatment procedure, clear evolution of the CsI peaks (marked with a green star) is observed. The simulated patterns for the dimer form (black) and CsI (green) are also provided. The inset shows an orange film of the dimer form of $Cs_3Sb_2I_9$ prepared by evaporating a stoichiometric mixture of reactants in acetonitrile.

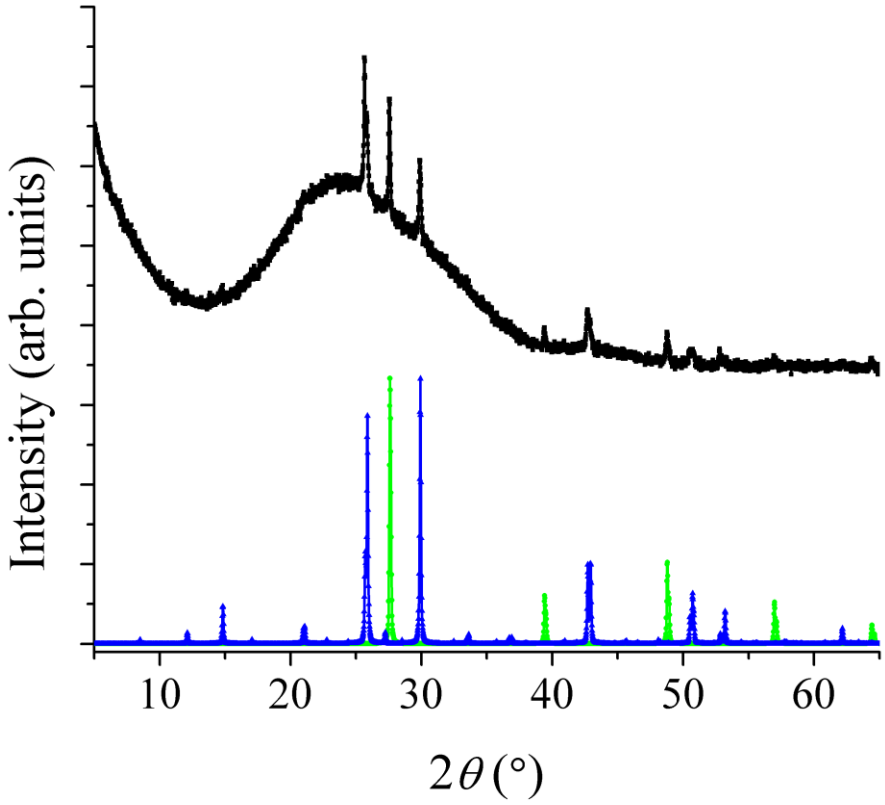

Figure S3. XRD pattern of a powder obtained from oriented $Cs_3Sb_2I_9$ films that are left in air for 6 months (black curve). The measurement on powdered films (i.e., scraped off of the substrate) confirms the presence of layered modification only, with CsI as the impurity phase. The broad background originates from the glass holder. The simulated patterns of the layered $Cs_3Sb_2I_9$ and CsI are shown in blue and green, respectively.

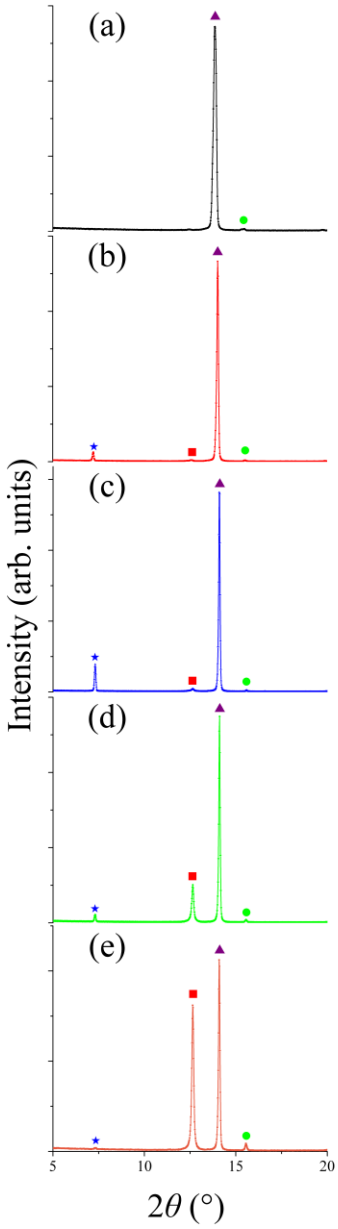

Figure S4. X-ray diffraction patterns of (a) a $CH_3NH_3PbI_3$ film exposed to ambient air with relative humidity ranging from 20 to 50% for (b) 2 weeks, (c) 3 weeks, (d) 4 weeks, and (e) for 60 days. $CH_3NH_3PbI_3$ (purple triangle) gradually decomposes forming hydrates of $CH_3NH_3PbI_3$ (blue star) and PbI_2 (red square). Since the $CH_3NH_3PbI_3$ film is prepared using $PbCl_2$ as a starting material, a small amount of leftover chlorides assemble into $CH_3NH_3PbCl_3$ impurity (green circle).

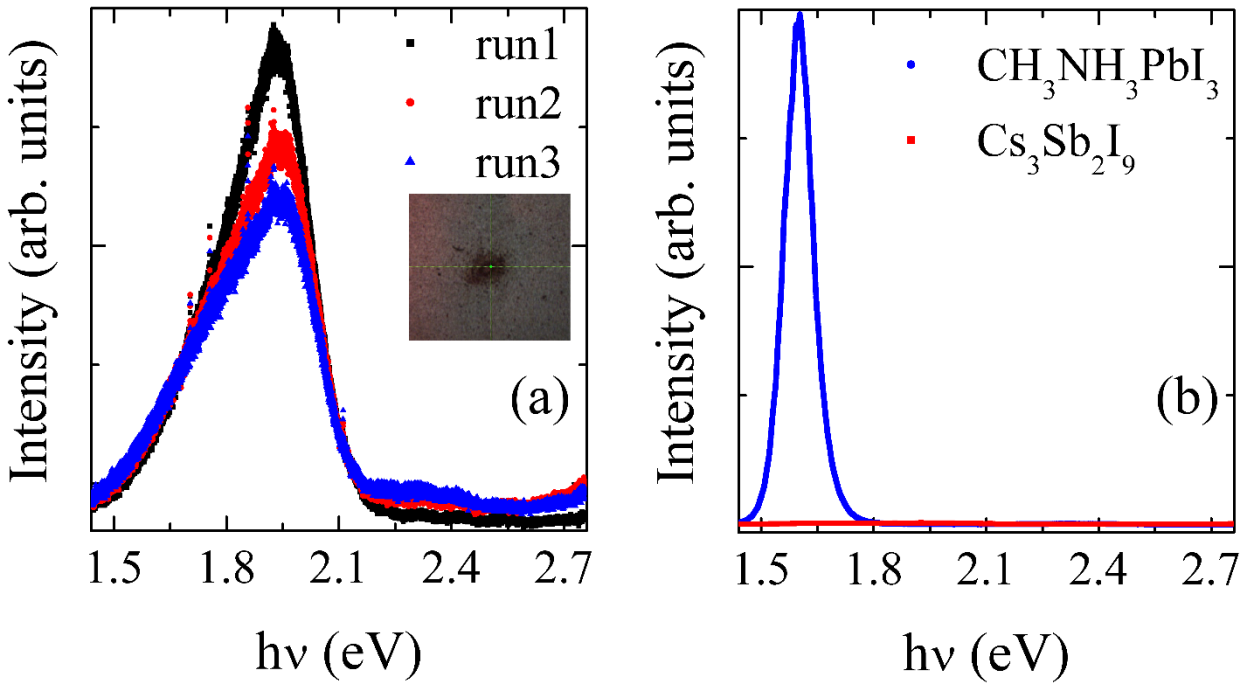

Figure S5. (a) Back-to-back photoluminescence (PL) measurements on the same spot leads to a gradual decrease of the PL peak for $Cs_3Sb_2I_9$ due to a decomposition of the film. The inset shows damage from the laser after several scans with longer exposure times. (b) A comparison of PL peak spectra for $CH_3NH_3PbI_3$ and $Cs_3Sb_2I_9$ films obtained under similar conditions.

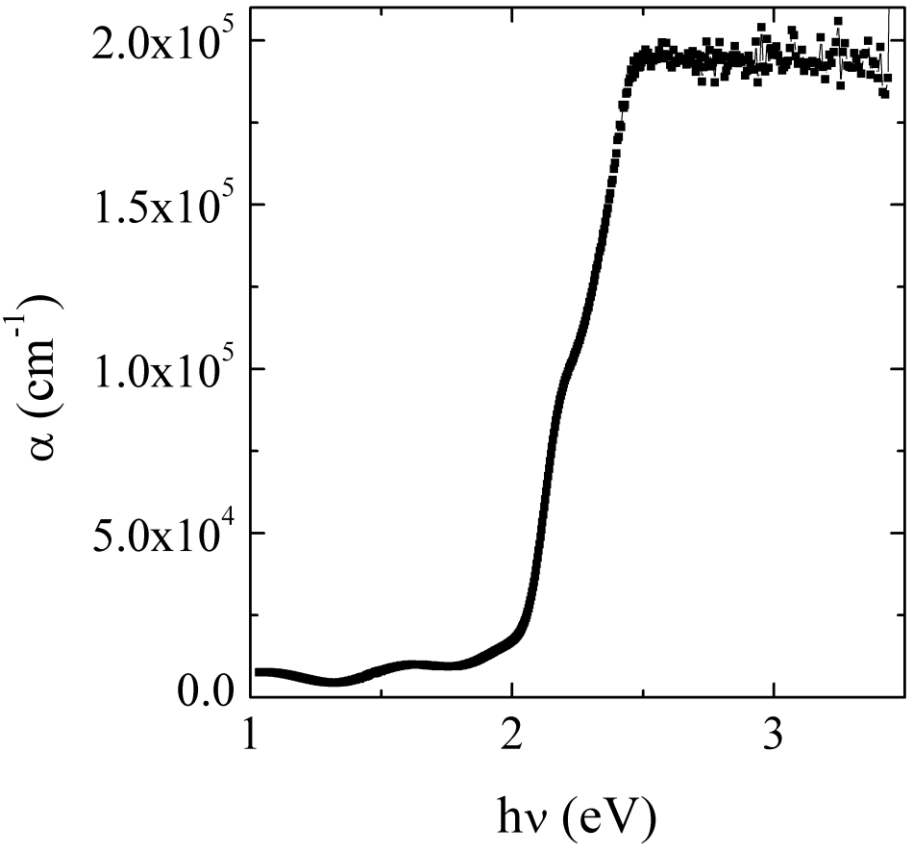

Figure S6. The energy dependence of the experimental absorption coefficient calculated from the absorption data provided in Figure 5 using Lambert's Law for a 440 nm thick film.

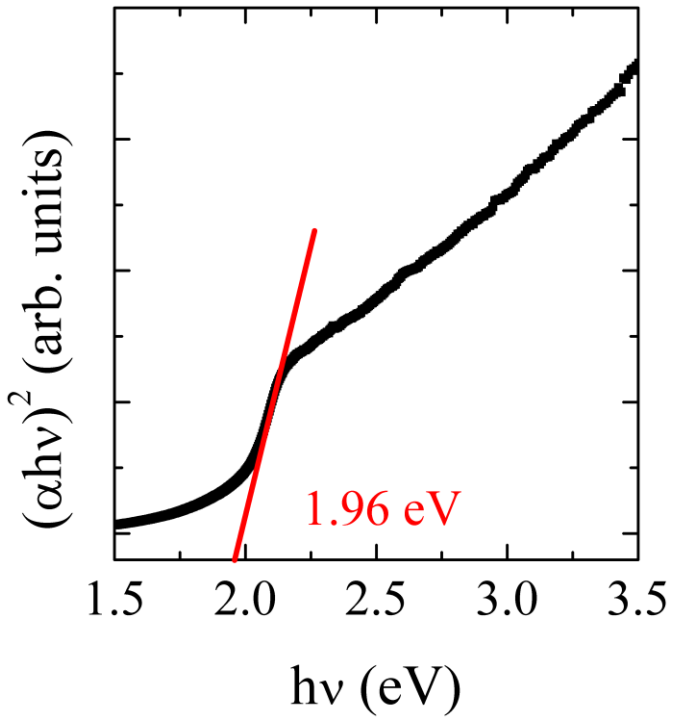

Figure S7. Optical absorption spectrum of a layered $Cs_3Sb_2I_9$ film left in moist air for 6 months.

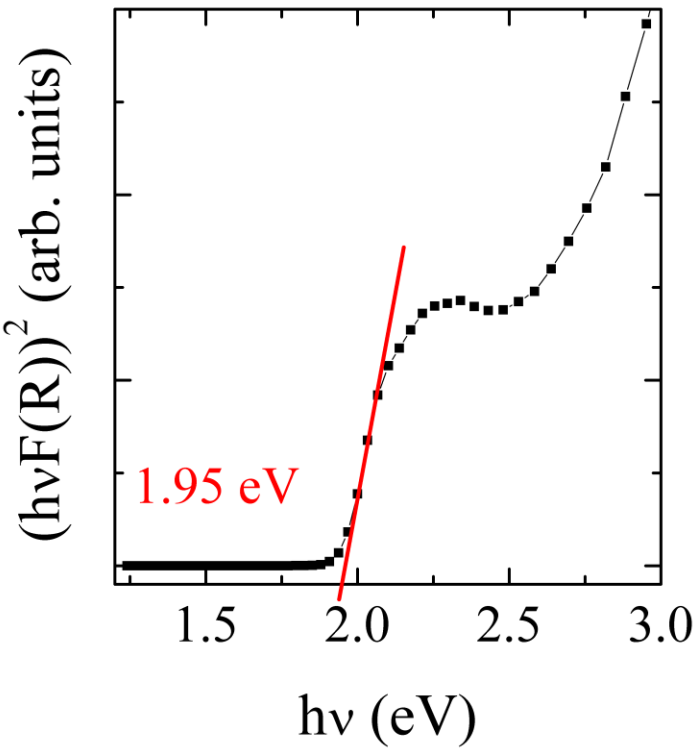

Figure S8. Diffuse reflectance data measured on a bulk sample of the layered $Cs_3Sb_2I_9$ gives a band gap of 1.95 eV. The Kubelka-Munk function, F(R), is proportional to the absorption coefficient, α. The band gap is obtained by substituting α with F(R) in the Tauc equation.

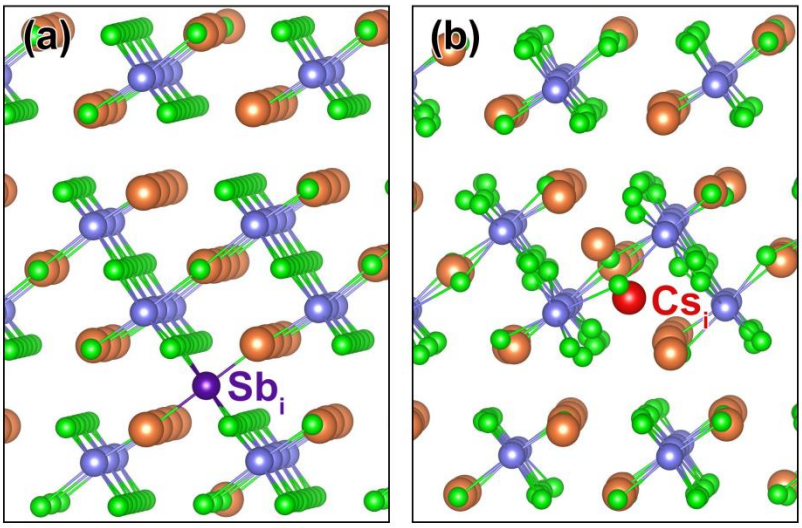

Figure S9. The atomic structures of the most stable configuration for (a) Sb_i and (b) Cs_i interstitials. The orange, blue, and green spheres represent Cs, Sb, and I atoms, respectively.

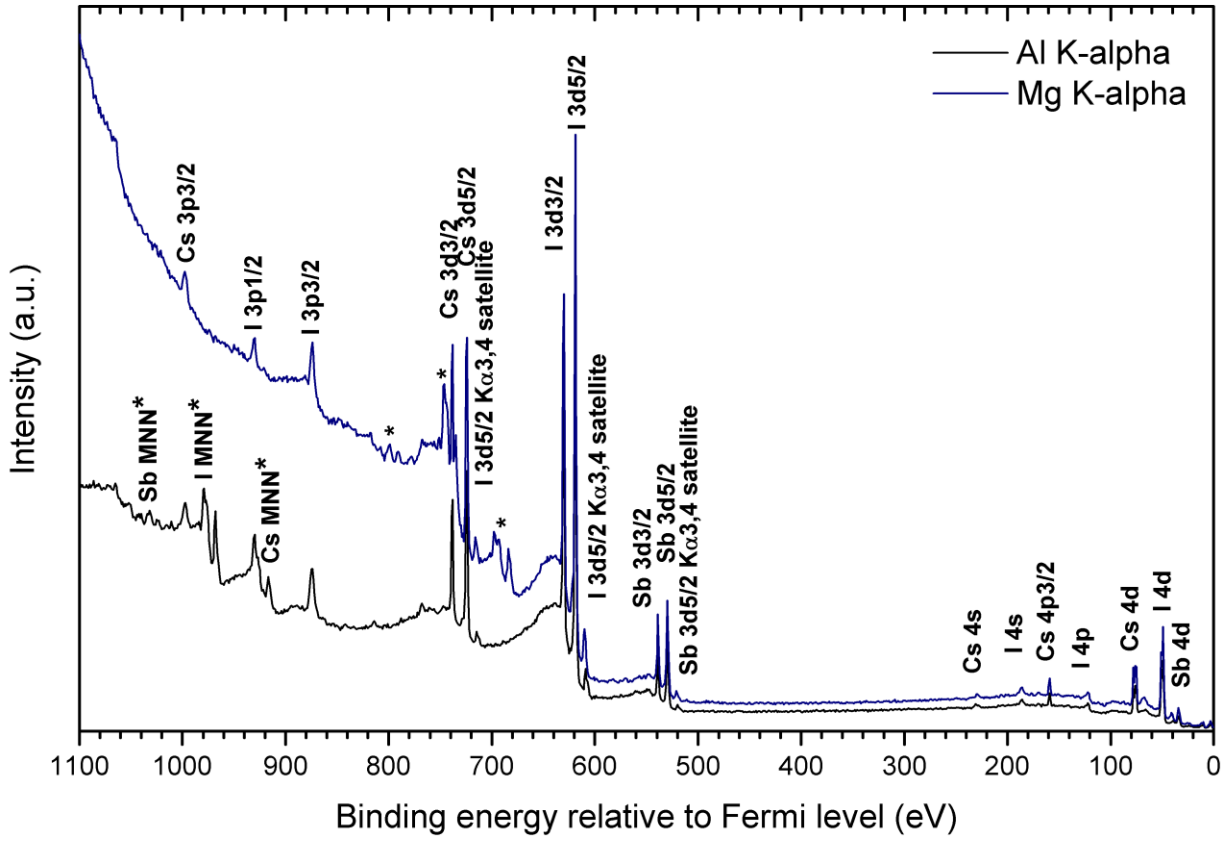

Figure S10. XPS Al and Mg Kα survey scans of the as-loaded 300 nm film. The peaks indicated with star (*) on the Mg Kα spectrum correspond to Auger MNN peaks. With the exception of C and O, no contaminants were detected in the as-loaded samples.

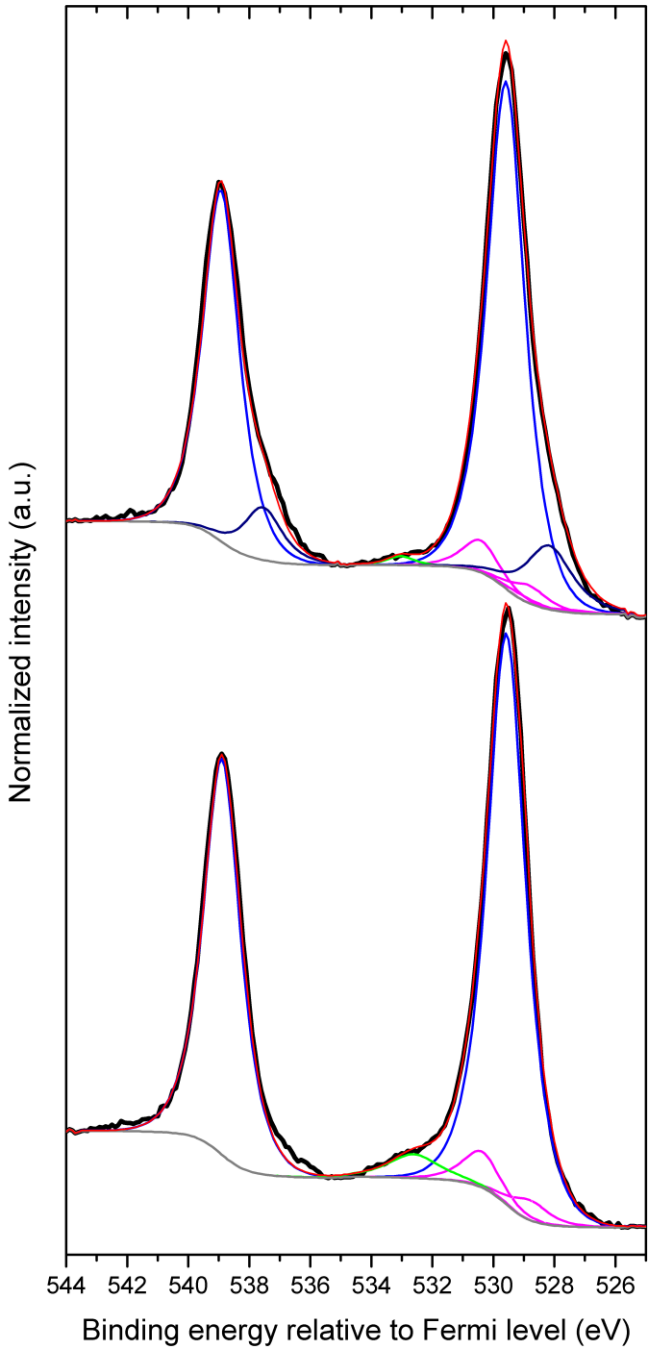

Figure S11. XPS Mg Kα close-up scan of the Sb 3d region (black), with Shirley background (grey), main 3d peaks (blue), satellites (magenta), oxygen 1s contribution (green) and sum of fitted peaks (red). The top and bottom spectra correspond to the 30 second-sputtered and as-loaded films, respectively.

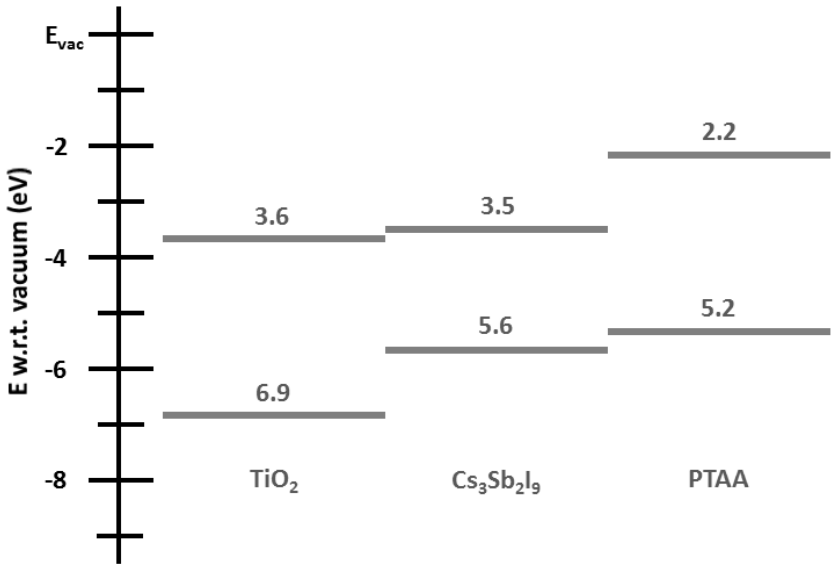

Figure S12. Energy band alignment between $Cs_3Sb_2I_9$, and c-TiO_2 and PTAA interfaces.

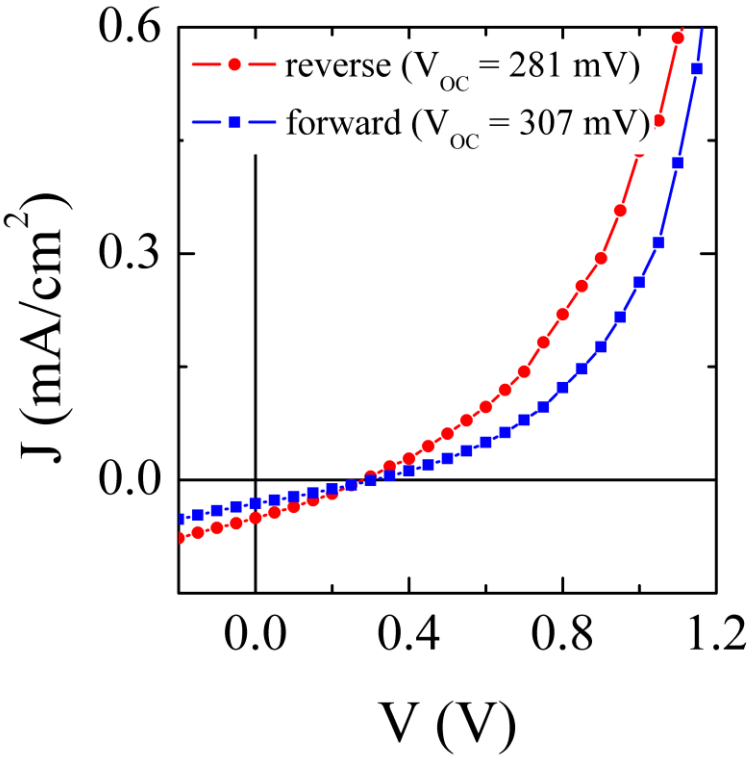

Figure S13. J-V curves for a representative solar cell based on the layered $Cs_3Sb_2I_9$ film as an absorber material. The forward and reverse scans were performed from -0.2 to 1.2 V and 1.2 to -0.2 V, respectively, with a 1s delay time.

Table S1. Elemental compositions of randomly-oriented layered $Cs_3Sb_2I_9$ films before and after sputtering is indicative of a gradual decomposition resulting in loss of the volatile SbI_3.

	Atomic Percentages (%)			Core Level Binding Energies (eV)		
	Cs	Sb	I	Cs $3d_{5/2}$	Sb $3d_{5/2}$*	I $3d_{5/2}$
Expected	21.4	14.3	64.3	--	--	--
As-loaded	24	15	61	724.29	529.54	618.76
30 second sputtering	27	13	60	724.31	529.59	618.77
5 minute sputtering	35	10	54	724.31	529.73	618.76
10 minute sputtering	34	11	55	724.48	529.80	618.90
	Error: Cs ± 2%, Sb ± 2%, I ± 3%			Error: ± 0.05 eV		

*Sb binding energy is for the high binding energy component (i.e. the peak present before sputtering)

References

(1) Yamada, K.; Sera, H.; Sawada, S.; Tada, H.; Okuda, T.; Tanaka, H. Reconstructive Phase Transformation and Kinetics of Cs3Sb2I9 by Means of Rietveld Analysis of X-Ray Diffraction and127I NQR. *J. Solid State Chem.* **1997,** *134*, 319-325.

(2) Sime, R. J. The vapor pressures and bond energies of some antimony halides. *J. Phys. Chem.* **1963,** *67*, 501-503.

(3) Bruner, B. L.; Corbett, J. D. A vapour-pressure study of the solution of antimony in liquid antimony (III) iodide—the formation of Sb2I4. *J. Inorg. Nucl. Chem.* **1961,** *20*, 62-65.

(4) Eperon, G. E.; Burlakov, V. M.; Docampo, P.; Goriely, A.; Snaith, H. J. Morphological Control for High Performance, Solution-Processed Planar Heterojunction Perovskite Solar Cells. *Adv. Funct. Mater.* **2014,** *24*, 151-157.

(5) Ha, S. T.; Liu, X.; Zhang, Q.; Giovanni, D.; Sum, T. C.; Xiong, Q. Synthesis of Organic–Inorganic Lead Halide Perovskite Nanoplatelets: Towards High-Performance Perovskite Solar Cells and Optoelectronic Devices. *Adv. Optical Mater.* **2014,** *2*, 838-844.

(6) Leguy, A. M. A.; Hu, Y.; Campoy-Quiles, M.; Alonso, M. I.; Weber, O. J.; Azarhoosh, P.; van Schilfgaarde, M.; Weller, M. T.; Bein, T.; Nelson, J.; Docampo, P.; Barnes, P. R. F. Reversible Hydration of CH3NH3PbI3 in Films, Single Crystals, and Solar Cells. *Chem. Mater.* **2015,** *27*, 3397-3407.

(7) Christians, J. A.; Miranda Herrera, P. A.; Kamat, P. V. Transformation of the Excited State and Photovoltaic Efficiency of CH3NH3PbI3 Perovskite upon Controlled Exposure to Humidified Air. *J. Am. Chem. Soc.* **2015,** *137*, 1530-1538.

(8) Hao, F.; Stoumpos, C. C.; Liu, Z.; Chang, R. P. H.; Kanatzidis, M. G. Controllable Perovskite Crystallization at a Gas–Solid Interface for Hole Conductor-Free Solar Cells with Steady Power Conversion Efficiency over 10%. *J. Am. Chem. Soc.* **2014,** *136*, 16411-16419.

(9) You, J.; Yang, Y.; Hong, Z.; Song, T.-B.; Meng, L.; Liu, Y.; Jiang, C.; Zhou, H.; Chang, W.-H.; Li, G.; Yang, Y. Moisture assisted perovskite film growth for high performance solar cells. *Appl. Phys. Lett.* **2014,** *105*, 183902.